Version: June 8, 2018
Preprint typeset using LaTeX style emulateapj v. 5/2/11

DISCOVERY OF A QUADRUPLE LENS IN CANDELS WITH A RECORD LENS REDSHIFT $Z = 1.53$

A. van der Wel[1], G. van de Ven[1], M. Maseda[1], H.W. Rix[1], G.H. Rudnick[2,1], A. Grazian[3], S.L. Finkelstein[4], D. C. Koo[5], S.M. Faber[5], H.C. Ferguson[6], A.M. Koekemoer[6], N.A. Grogin[6], D.D. Kocevski[7]

Version: June 8, 2018

ABSTRACT

Using spectroscopy from the *Large Binocular Telescope* and imaging from the *Hubble Space Telescope* we discovered the first strong galaxy lens at $z_{\rm lens} > 1$. The lens has a secure photometric redshift of $z = 1.53 \pm 0.09$ and the source is spectroscopically confirmed at $z = 3.417$. The Einstein radius (0.35"; 3.0 kpc) encloses 7.6×10^{10} $M_\odot$, with an upper limit on the dark matter fraction of 60%. The highly magnified (40×) source galaxy has a very small stellar mass ($\sim 10^8$ $M_\odot$) and shows an extremely strong $[\mathrm{OIII}]_{5007\mathring{A}}$ emission line ($EW_0 \sim 1000$Å) bolstering the evidence that intense starbursts among very low-mass galaxies are common at high redshift.

1. INTRODUCTION

Strongly lensing galaxies provide a range of important applications, from the measurement of cosmological parameters through time delays between lensed images (Refsdal 1964), to the direct measurement of total galaxy masses (e.g., Kochanek 1995), to the evolution and ages of elliptical galaxies (e.g., Rusin et al. 2003; van de Ven et al. 2003), to the radial profile of the dark matter distribution (e.g., Treu & Koopmans 2004).

Since the discovery of the first $z = 1$ strong lens almost 30 years ago (Lawrence et al. 1984; Schneider et al. 1986), no strong lenses at higher redshifts have been found, despite the large number of $z \lesssim 1$ lenses discovered since then (e.g., Bolton et al. 2006; Faure et al. 2008; More et al. 2012), and a handful of tentative $z \sim 1.2$ candidates (More et al. 2012) for which the lens nature is unfortunately doubtful.

The paucity of $z > 1$ lenses has four causes: first, lensing probabilities decrease for lenses at higher redshifts due to the small relative distances between lenses and sources – for example, the Einstein radius for a $\sigma = 200$ km s^{-1} galaxy at $z = 1.5$ is only ~ 0.4" for a $z > 2.5$ source. Second, the reduced volume and number density of sources behind potential lenses is greatly reduced. Third, massive galaxies are increasingly rare at higher redshifts, and those with the highest lensing probability – the most concentrated, bulge-dominated galaxies – are usually red and faint in the rest-frame ultraviolet and hence in optical $z > 1$ surveys. Fourth, the measurement of lens and source redshifts and the confirmation of the lens nature require near-infrared spectroscopy, which has been much more challenging than optical spectroscopy.

Based on the number counts of potential high-redshift ($z > 2.5$) sources (e.g., Bouwens et al. 2007) and the $z = 1 - 2$ mass function of potential lenses (e.g., Ilbert et al. 2010; Brammer et al. 2011) we estimate one $z > 1$ galaxy-galaxy lens to occur per ~ 200 square arcminutes. Thus, large-area, near-infrared surveys are needed to have any chance to find $z > 1$ lenses: the largest current survey of this kind, CANDELS (Grogin et al. 2011; Koekemoer et al. 2011), covers 800 square arcminutes with *Hubble Space Telescope* near-infrared imaging, such that it should contain a handful of $z > 1$ lenses with background sources intrinsically brighter than 28th magnitude (AB) in the near-infrared.

Here we present the discovery of the quadruple galaxy-galaxy lens J100018.47+022138.74 (J1000+0221) using imaging data from CANDELS and near-infrared spectroscopy from the *Large Binocular Telescope* (LBT). We report a spectroscopically confirmed source redshift of $z_S = 3.417 \pm 0.001$ and a record lens galaxy redshift of $z_L = 1.53 \pm 0.09$.

The $z = 1.53$ lens is a flattened, quiescent galaxy with a stellar mass of $\sim 6 \times 10^{10}$ $M_\odot$ and appears to be located in a previously unknown overdense region populated with at least a half a dozen of L^* galaxies at the same redshift. Its Einstein radius of 0.35" (3.0 kpc at $z = 1.53$) presents us with the first opportunity for a direct mass measurement in this redshift range through lensing, providing an important confirmation of previous results based on stellar absorption line kinematics (see, e.g., van de Sande et al. 2013, and references therein), which has been technically challenging.

2. DATA

CANDELS *HST*/Wide Field Camera 3 (WFC3, Kimble et al. 2008) (F125W+F160W) and HST/Advanced Camera for Surveys (ACS, Ford et al. 2003) (F606W+F814W) imaging of the lens+source system is shown Figure 1. The false-color image shows the unambiguous lens nature of J1000+0221: the four blue images at a sub-arcsecond scale surrounding a red galaxy are a tell-tale sign. Before generating the color map each individual image was deconvolved with

[1] Max-Planck Institut für Astronomie, Königstuhl 17, D-69117, Heidelberg, Germany; e-mail:vdwel@mpia.de
[2] Department of Physics and Astronomy, The University of Kansas, Malott room 1082, 1251 Wescoe Hall Drive, Lawrence, KS 66045, USA
[3] INAF - Osservatorio Astronomico di Roma, via Frascati 33, 00040, Monteporzio, Italy
[4] Department of Astronomy, The University of Texas at Austin, Austin, TX 78712, USA
[5] UCO/Lick Observatory, Department of Astronomy and Astrophysics, University of California, Santa Cruz, CA 95064, USA
[6] Space Telescope Science Institute, 3700 San Martin Drive, Baltimore, MD 21218, USA
[7] Department of Physics and Astronomy, University of Kentucky, 505 Rose Street, Lexington, Kentucky 40506, USA

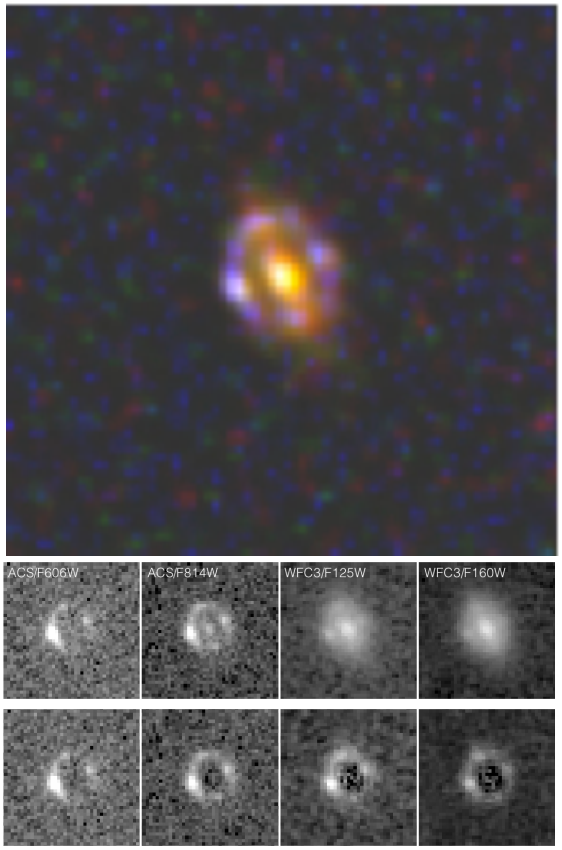

Figure 1. *Top*: Quadruple gravitational lens J1000+0221 with an Einstein radius of 0.35". The false-color image is generated using HST/WFC3 imaging from CANDELS (F125W in green, and F160W in red) and HST/ACS imaging from COSMOS and CANDELS (F814W in blue). These individual images were processed with the Lucy-Robertson deconvolution algorithm. The lensing galaxy is a flattened galaxy with little or no star formation and a stellar mass of $\sim 6 \times 10^{10}$ $M_\odot$. Its redshift of $z = 1.53 \pm 0.09$ makes this galaxy the most distant strong galaxy lens discovered to date. The source, magnified by a factor 40, is a young, strongly starbursting galaxy with a very small stellar mass ($\sim 10^8$ $M_\odot$). *Bottom:* HST/ACS and HST/WFC3 images (2.4"×2.4") of the lens-source system (top row). A Sérsic model is produced based on the F160W image, masking the annulus containing the source images. This Sérsic model is scaled and subtracted from the other images. The residuals are shown in the bottom row.

the Lucy-Robertson algorithm, using appropriate point spread functions (PSFs) for each filter (§3). Images in the individual filters are shown in Figure 1. Especially after subtraction of the lens (see §3 for details) the almost continuous Einstein ring with a radius of ~ 0.35" is clearly seen in all filters.

The source redshift $z_S = 3.417$ is measured from LBT/LUCI (Seifert et al. 2003) near-infrared spectroscopy originally aimed at obtaining continuum spectroscopy of massive galaxies at $z = 1.5 - 2$. A 3-hour observing sequence of individual, dithered 120s exposures with the H+K grism in a 1" wide slit and seeing ∼0.6" produced significant detections of three emission lines in the K band, identified as H_β and 2× [OIII] (see Figure 2). These fortuitously lensed emission lines allowed us to identify the lens nature of the system, which we were able to confirm upon visual inspection of the HST imaging described above. No spectroscopic redshift for the lens could be determined from the H- or K-band spectrum. The multi-slit capability of LUCI allowed us to

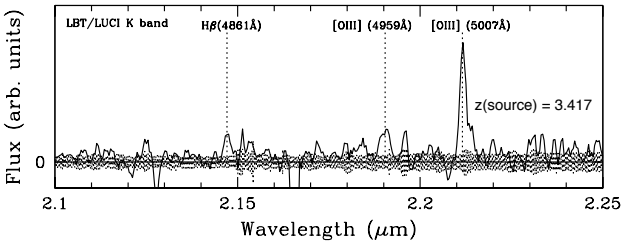

Figure 2. LBT/LUCI K-band spectrum of J1000+0221, smoothed with the instrumental resolution. The marginally non-zero continuum is mostly due to the $z = 1.53$ lens. The three indicated nebular emission lines, all detected with 10σ confidence or better, are from the source at $z = 3.417$. The strength of the emission line galaxies and [OIII]/Hβ line ratio imply a very young (10 Myr), star-bursting system. Given the magnification of $\mu = 40$, we infer a stellar mass of $\sim 10^8$ $M_\odot$.

target several of the galaxies in the immediate vicinity of J1000+0221, one of which we spectroscopically confirmed at $z = 1.525$ through the detection Hα and [NeIII] in the H band. The LUCI data reduction procedure is described in detail by M. Maseda et al. (in prep.).

Finally, we include ground-based photometry in our analysis. We use the Newfirm Medium Band Survey (NMBS) multi-wavelength catalog and derived data products from Whitaker et al. (2011), as well as *Ugr* LBT photometry from the *Large Binocular Cameras* (LBC, Boutsia et al. in prep.). These datasets provide us with combined photometry for the lens and source, which we will jointly analyze with the spatially separated photometry from the HST data described in §3 in order to obtain accurate redshift and stellar mass estimates.

3. LENS-SOURCE IMAGE DECOMPOSITION

We use `GALFIT` (Peng et al. 2010) and the PSF from van der Wel et al. (2012) to produce a Sérsic model for the F160W image of the lens. An annulus with an inner radius of 0.18" and an outer radius of 0.66" containing the source images is masked in the fitting process. The half-light radius measured along the major axis is $R_{\rm eff} = 0.29 \pm 0.01$" or $R_{\rm eff} = 2.5 \pm 0.1$ kpc. The Sérsic index is $n = 2.2 \pm 0.2$, the projected axis ratio $q = 0.52 \pm 0.01$, and the position angle ($PA = 27 \pm 1$ degrees from North to East). The results do not significantly change if the masked region is made narrower. This size and shape are rather typical for early-type galaxies at $z \sim 1.5$ (e.g., van der Wel et al. 2011; Chang et al. 2013).

Then, for each of the ACS and WFC3 images, we convolve this Sérsic model with the appropriate PSF model[8] and scale the total flux to minimize the residual flux within a radius of 0.18". The scaled models provide us with PSF-matched photometry of the lens. The lens-subtracted images are shown in the bottom row of Figure 1. Total source fluxes are then measured within 1" diameter apertures.

In order to increase the wavelength coverage, we take the IRAC 3.6μm and 4.5μm photometry from the NMBS

[8] The F125W PSF is taken from van der Wel et al. (2012); a bright, non-saturated star in the mosaic serves as the PSF model for the ACS images.

Table 1
Photometry based on decomposed HST images (Figure 1) and Spitzer/IRAC photometry.

	F606W	F814W	F125W	F160W	$IRAC_{3.6}$	$IRAC_{4.5}$	z
	AB mag						
lens	26.4±0.4	25.3±0.2	22.43±0.05	21.85±0.05	20.9±0.1	20.8±0.1	1.53±0.09
source	24.3±0.1	23.8±0.1	23.9±0.2	23.9±0.3	···	···	3.417±0.001

Table 2
Positions and flux ratios of lens and images. The positional uncertainty is 10^{-5} degrees.

	R.A. J2000	Dec. J2000	F160W flux ratio Arb. units
lens	150.0769694	+2.3607623	···
image A	150.0770240	+2.3608697	0.37±0.03
B	150.0768853	+2.3607955	0.30±0.03
C	150.0770630	+2.3607356	0.69±0.04
D	150.0769501	+2.3606752	0.14±0.03

catalog and include a small correction for the source flux, estimated to be 10% based on the spectral energy distribution of the source (see §6). Hence we have obtained separate photometry for the lens and the source, which we show in Figure 3 and list in Table 1.

4. LENS REDSHIFT AND STELLAR MASS

Spectroscopic confirmation of the lens redshift has remained elusive due to its faintness ($V \sim 26$; $H_{\rm F160W} \sim 22$) and apparent lack of emission lines. However, the red $I_{F814W} - J_{F125W}$ color implies the presence of the Balmer and/or 4000Å break straddled by these two filters, suggesting a redshift in the range $1.2 < z < 2.0$. Using `EAZY` (Brammer et al. 2008) we construct the redshift probability distribution based on the photometry given in Table 1, and find that the peak lies at $z = 1.53$. We find the same result if we include the LBC U-band photometry.

The lens-source system is unresolved in the ground-based imaging, which thus produces the sum of the fluxes of the source and the lens. The source has an accurately known redshift and a very simple spectral energy distribution (SED), given that it is young and dust-poor as indicated by the blue colors (see Figure 3 and §6). The `EAZY` redshift probability distribution for the lens based on the NMBS photometry after subtracting the source SED peaks at $z = 1.50$. The combined probability distribution from the two independent redshift estimates give $1.44 < z < 1.62$ ($1.34 < z < 1.74$) as the 68% (95%) confidence interval, with no secondary redshift solutions.

Further credence to our redshift estimate of the lens, and the precise value of $z = 1.53$ in particular, is lent by the four $\sim 10^{11}$ $M_\odot$ galaxies with $z_{\rm phot} \sim 1.5$ in the NMBS catalog within a projected distance of 250 kpc, one of which could be spectroscopically confirmed at $z = 1.525$ with our LUCI spectroscopy. This is the only such overdensity in the COSMOS field, and suggests that the lens is a member.

We use `FAST` (Kriek et al. 2009) to estimate the lens stellar mass, star-formation history and attenuation based on the ACS+WFC3+IRAC photometry given in Table 1. The best-fitting, solar metallicity model, shown in red in Figure 3, has an age of 1 Gyr, with an exponentially declining star formation rate ($\tau = 0.05$ Gyr), and moderate extinction (A_V=0.8). Dustier models with some residual star formation cannot be ruled out. The star formation rate is at most a few $M_\odot$ / yr^{-1} given that we see no Hα in the LUCI spectrum and only have a marginally significant Spitzer 24μm flux (from the NMBS catalog). The stellar mass is $M_* = 6^{+4}_{-1} \times 10^{10}$ $M_\odot$, assuming a Chabrier (2003) stellar initial mass function. Although the results of the SED fit suffer from the usual age-metallicity degeneracy, the mass estimate is not sensitive to departures from the adopted (solar) metallicity.

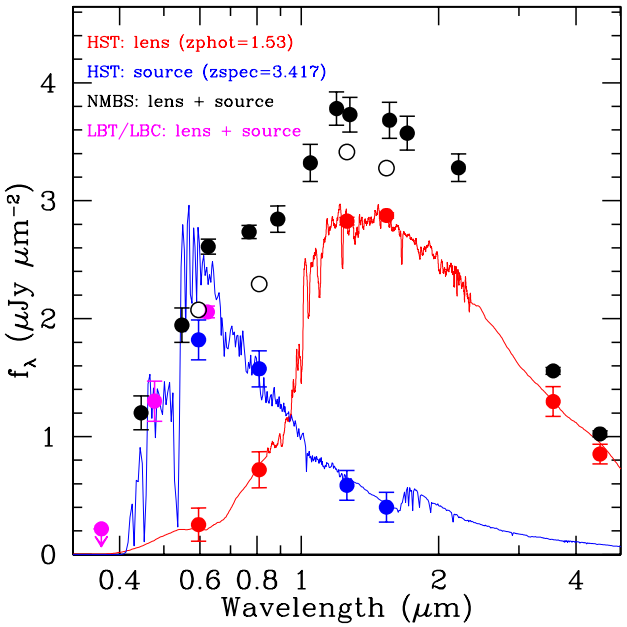

Figure 3. Spectral energy distribution of gravitational lens system J1000+0221. The blue points show the HST photometry of the source, derived from the lens-subtracted images shown in Figure 1; the red points show the HST photometry of the lens, obtained from `GALFIT`-based Sérsic models for the lens; the open black points show the sum of the HST photometry for lens and source; the filled black points show ground-based photometry for the combined lens-source system from NMBS (Whitaker et al. 2011); the magenta points show ground-based photometry for the combined lens-source system from LBT/LBC (Boutsia et al. (in prep.). The LBT/LBC fluxes r-band flux agrees very well with the HST F606W flux. The offset between the NMBS photometry on the one hand, and the HST and LBT photometry on the other hand is of unknown origin. The red and blue lines are spectral energy distributions that represent acceptable fits to the photometry of the lens and source, respectively. The source model is a dust-free, 50 Myr old single stellar population (see §6). The lens model has exponentially declining star formation rate with an age of 1 Gyr and $A_V = 0.8$ (see §4).

5. LENS MODEL

We use the method described by van de Ven et al. (2010) to produce an analytical lens model that allows for a non-spherical underlying mass distribution. In Table 2 we provide the coordinates of the lens center and the four source images, as well as flux ratios for the images measured in F160W. The flux ratios vary with wavelength, as is immediately apparent from the the lens-subtracted

images shown in Figure 1: the brightest image is also the bluest. We rule out a supernova by examining the ACS images at two different epochs, such that the color variations suggest that the source has intrinsic, spatial color variations, or that there is dust in the lens, the distribution of which is patchy. Because of the color variations we do not use the flux ratios of the images in our lensing model. Our best-fitting lens model has an Einstein radius of $R_E = 0.35$" (or 3.0 kpc) with an enclosed mass of $M_E = (7.6 \pm 0.5) \times 10^{10}\ M_\odot$. The total magnification of the source, which is aligned almost perfectly (to within 0.01") with the lens, is $\mu = 40 \pm 2$.

Given that 66% of the F160W light from the lens falls within the Einstein radius we derive a stellar mass within the Einstein radius of $M_*(< R_E) = 4^{+2}_{-1} \times 10^{10}\ M_\odot$, which implies that stars likely account for the majority, but not necessarily all, of the mass within R_E. This is also the case if we increase the stellar mass by adopting the Salpeter IMF (which cannot be ruled out) rather than the Chabrier IMF. An indication that light does not precisely trace mass is that the (tangential) critical curve for a mass distribution that is as flattened as the observed light distribution should also be somewhat elongated (in the direction perpendicular to that of the light distribution). The image configuration, however, implies that critical curve is very close to circulur. Furthermore, if mass follows light, then the implied mass profile at R_E is unusually steep: with little scatter, the typical slope is known to be close to isothermal ($\gamma \sim 2$, Koopmans et al. 2009), whereas the implied slope here is $\gamma \sim 3$. Given our stellar mass estimate, the roundness of the critical curve, and the extremely steep mass profile slope inferred under the assumption that mass follows light, we conclude that there likely is a significant contribution from dark matter within R_E of the lens, with an 1-σ upper limit of 60%.

As described above, the lens is situated in an overdense environment, which likely contributes to the projected, enclosed mass. A crude estimate of this effect can be inferred by assuming that the most massive galaxy in the overdensity, which lies at a projected distance of 110 kpc, is situated at the center of a spherical Navarro et al. (1996) dark matter halo with concentration parameter $c = 6$. Based on the stellar mass of this central galaxy ($M_* = 3 \times 10^{11}\ M_\odot$) we estiamte the halo to have a total mass of $10^{13.5-14} M_\odot$ (Moster et al. 2013), such that the projected mass within the Einstein radius of the lens is $\sim 10^{10}\ M_\odot$. This does not significantly affect our conclusions regarding the dark matter and stellar mass fractions.

Finally, we note that the velocity dispersion implied by the lens model ($\sqrt{M_E/R_E} \equiv \sigma_E = 182 \pm 10$ km s^{-1}) is consistent with stellar velocity dispersions of galaxies at similar redshifts as measured from absorption line spectra (e.g., van de Sande et al. 2013, and references therein): the velocity dispersion is higher by $\sim 20\%$ compared to present-day galaxies with a similar mass. Our accurate and precise measurement of the velocity dispersion provides important support to the results based on stellar kinematics given the practical difficulties associated with continuum spectroscopy for $z \gtrsim 1.5$ galaxies.

6. NATURE OF THE SOURCE

The HST photometry of the source (blue points in Figure 3) shows a very blue continuum, indicative of a young, dust-free galaxy. Using the method described by Finkelstein et al. (2012) we fit the spectral energy distribution given by the four photometric data points (F606W, F814W, F125W, and F160W) given in Table 1. We confirm the young age (50 ± 30 Myr), dust-free nature ($E(B-V) = 0.00^{+0.16}_{-0.00}$), and blue continuum slope ($\beta = -2.0 \pm 0.3$) of the source. The (de-magnified) stellar mass of the galaxy is $M_* = 2.6^{+2.0}_{-1.3} \times 10^8\ M_\odot$. The best-fitting model spectral energy distribution is shown in Figure 3.

As we mentioned above and showed in Figure 2, three emission lines are detected with high significance: Hβ and [OIII] at 4959Å and 5007Å. We detect a low-level (1-2σ per pixel) continuum in the spectrum, and we use the average continuum flux over the entire K-band wavelength range to estimate the equivalent width of the brightest [OIII] line at $EW([OIII]_{5007\text{Å}}) = 340 \pm 50$Å in the observed frame, or $EW_0([OIII]_{5007\text{Å}}) = 77 \pm 11$Å in the rest-frame of the source[9]. Adopting the K band flux ratio predicted by the SED models for the source and the lens we arrive at an estimated rest-frame $EW_0([OIII]_{5007\text{Å}}) = 1200 \pm 300$Å for the source alone.

This high EW is consistent with the stellar population properties estimates above, although we note that this is not necessarily the EW of the unlensed source, as a spatially varying EW could lead to a boosted, lensed EW. The fact that the brightest image is also the bluest may indicate that this may be the case here, but it is beyond the scope of our analysis to attempt to correct for this effect.

The [OIII]/Hβ line ratio from the spectrum shown in Figure 2 is 5^{+2}_{-1}, indicative of a high excitation, and likely a low metallicity. Additional emission lines such as [OII] or [NeIII], needed to confirm the low metallicity, are not detected.

An abundant population of objects at $z \sim 2$ with very high [OIII] EW_0 was identified by van der Wel et al. (2011), and the properties of those extreme emission line galaxies are very similar to those of the source described here (also see Atek et al. 2011). Remarkably, this is the second such emission-line dominated object that is found to be strongly lensed in CANDELS: using data from the 3D-HST survey (Brammer et al. 2012a), Brammer et al. (2012b) found a galaxy at $z_S = 1.847$ with very similar mass and age. Given the abundance of unlensed emission-line galaxies it was seemingly unlikely that even one strongly lensed version exists within a CANDELS-sized survey. The existence of two strong lensed galaxies of this kind suggests that such galaxies are likely even more common than is currently assumed, and that objects near or below the detection limits of current surveys – the unlensed magnitude of the $z = 3.417$ source is $H_{\text{F160W}} \sim 28$ – very commonly display such strong emission lines (*cf.*, Smit et al. 2013). This would have profound consequences for our understanding of galaxy formation: a presumably brief burst of intense star formation may signal the initial formation stage of any galaxy.

[9] The lens+source system is smaller than the slit width, as is the seeing disk for our observations, such that slit losses are negligible.

Euclid will reveal tens of thousands $z > 1$ lens candidates, which will give us unprecendented insight into the variety in properties among faint, high-redshift galaxies, as well as the galaxy mass function at all redshifts $0 < z < 2$ with perfectly calibrated mass measurements in an absolute sense.

The authors thank Ricardo Amorin, Marcello Cacciato, Nimish Hathi, David Koo, Ray Lucas, Sharon Meidt, Mara Salvato, Benjamin Weiner, and Steven Willner for helpful comments and suggestions. GHR acknowledges the support of an Alexander von Humboldt Foundation Fellowship for Experienced Researchers.

REFERENCES

Atek, H., Siana, B., Scarlata, C., et al. 2011, ApJ, 743, 121
Bolton, A. S., Burles, S., Koopmans, L. V. E., Treu, T., & Moustakas, L. A. 2006, ApJ, 638, 703
Bouwens, R. J., Illingworth, G. D., Franx, M., & Ford, H. 2007, ApJ, 670, 928
Brammer, G. B., van Dokkum, P. G., & Coppi, P. 2008, ApJ, 686, 1503
Brammer, G. B. et al. 2011, ApJ, 739, 24
Brammer, G. B. et al. 2012b, ApJ, 758, L17
Brammer, G. B. et al. 2012a, ApJS, 200, 13
Chabrier, G. 2003, PASP, 115, 763
Chang, Y.-Y. et al. 2013, ApJ, in press, arXiv:1305.6931
Faure, C. et al. 2008, ApJS, 176, 19
Finkelstein, S. L., Papovich, C., Salmon, B., et al. 2012, ApJ, 756, 164
Ford, H. C. et al. 2003, Proc. SPIE, 4854, 81
Grogin, N. A. et al. 2011, ApJS, 197, 35
Ilbert, O. et al. 2010, ApJ, 709, 644
Kimble, R. A., MacKenty, J. W., O'Connell, R. W., & Townsend, J. A. 2008, Proc. SPIE, 7010,
Kriek, M. et al. 2009, ApJ, 700, 221
Kochanek, C. S. 1995, ApJ, 445, 559
Koekemoer, A. M. et al. 2011, ApJS, 197, 36
Koopmans, L. V. E. et al. 2009, ApJ, 703, L51
Lawrence, C. R., Schneider, D. P., Schmidt, M., et al. 1984, Science, 223, 46
Leitherer, C. et al. 1999, ApJS, 123, 3
More, A. et al. 2012, ApJ, 749, 38
Moster, B. P., Naab, T., & White, S. D. M. 2013, MNRAS, 428, 3121
Navarro, J. F., Frenk, C. S., & White, S. D. M. 1996, ApJ, 462, 563
Peng, C. Y., Ho, L. C., Impey, C. D., & Rix, H.-W. 2010, AJ, 139, 2097
Refsdal, S. 1964, MNRAS, 128, 307
Rusin, D. et al. 2003, ApJ, 587, 143
Schneider, D. P. et al. 1986, AJ, 91, 991
Seifert, W. et al. 2003, Proc. SPIE, 4841, 962
Smit, R., Bouwens, R. J., Labbe, I., et al. 2013, arXiv:1307.5847
Treu, T., & Koopmans, L. V. E. 2004, ApJ, 611, 739
van de Sande, J. et al. 2013, ApJ, 771, 85
van der Wel, A. et al. 2011, ApJ, 730, 38
van der Wel, A. et al. 2011, ApJ, 742, 111
van der Wel, A. et al. 2012, ApJS, 203, 24
van de Ven, G., van Dokkum, P. G., & Franx, M. 2003, MNRAS, 344, 924
van de Ven, G. et al. 2010, ApJ, 719, 1481
Whitaker, K. E. et al. 2011, ApJ, 735, 86